NASA TECHNICAL MEMORANDUM

NASA TM X-2356

NASA TM X-2356

INFLIGHT THRUST MEASURING SYSTEM FOR UNDERWING NACELLES INSTALLED ON A MODIFIED F-106 AIRCRAFT

by Harold W. Groth, Nick E. Samanich, and Philip Z. Blumenthal

Lewis Research Center
Cleveland, Ohio 44135

NATIONAL AERONAUTICS AND SPACE ADMINISTRATION • WASHINGTON, D. C. • AUGUST 1971

1. Report No.	2. Government Accession No.	3. Recipient's Catalog No.
NASA TM X-2356		

4. Title and Subtitle	5. Report Date
INFLIGHT THRUST MEASURING SYSTEM FOR UNDERWING NACELLES INSTALLED ON A MODIFIED F-106 AIRCRAFT	August 1971
	6. Performing Organization Code

7. Author(s)	8. Performing Organization Report No.
Harold W. Groth, Nick E. Samanich, and Philip Z. Blumenthal	E-5557
	10. Work Unit No. 720-03

9. Performing Organization Name and Address	11. Contract or Grant No.
Lewis Research Center National Aeronautics and Space Administration Cleveland, Ohio 44135	
	13. Type of Report and Period Covered Technical Memorandum

12. Sponsoring Agency Name and Address	14. Sponsoring Agency Code
National Aeronautics and Space Administration Washington, D. C. 20546	

15. Supplementary Notes

16. Abstract

An F-106 aircraft was modified for use as a flight test bed to evaluate powerplant system performance using two underwing nacelles containing afterburning J85-13 engines. A calibration program was conducted to determine the random error of the thrust measuring system in evaluating flight performance of exhaust nozzles. The random error in the determination of a nacelle tare drag was nearly Gaussian and provided a repeatability of ±1.0 percent in the calculation of nozzle performance for 68 percent of the data.

17. Key Words (Suggested by Author(s))	18. Distribution Statement
Airframe installation effects; Airframe nacelle integration; Propulsion system; Transonic, underwing nacelles; Flight test; Nozzle installation	Unclassified - unlimited

19. Security Classif. (of this report)	20. Security Classif. (of this page)	21. No. of Pages	22. Price*
Unclassified	Unclassified	32	$3.00

*For sale by the National Technical Information Service, Springfield, Virginia 22151

INFLIGHT THRUST MEASURING SYSTEM FOR UNDERWING NACELLES INSTALLED ON A MODIFIED F-106 AIRCRAFT

by Harold W. Groth, Nick E. Samanich, and Philip Z. Blumenthal

Lewis Research Center

SUMMARY

An F-106 aircraft was modified for use as a flight test bed to evaluate powerplant system performance using two underwing nacelles containing afterburning J85-13 engines. A calibration program was conducted to determine tare forces and the random error of the thrust measuring system in evaluating flight performance of exhaust nozzles. It was conducted over a flight Mach number range from 0.60 to 1.30 and power settings from part power to maximum afterburning.

The procedure used to determine exhaust nozzle performance was shown to be feasible and repeatable. The system makes use of a calibrated nacelle tare force which is used in conjunction with a load cell reading to calculate nozzle performance. The random error in the determination of nacelle tare force was nearly Gaussian and resulted in repeatability of ±1.0 percent in the calculation of nozzle performance for 68 percent of the data.

INTRODUCTION

As a part of a research program to investigate installation effects upon various turbojet engine exhaust nozzles, a flight test program was initiated at Lewis Research Center. The flight program not only supplemented wind tunnel investigations but provided additional data in the transonic range where tunnels suffer from wall interference problems due to blockage effects and shock reflections. The flight program also allowed much larger scale research hardware to be investigated. The test program was conducted on an F-106 aircraft modified to permit installation of two pod-mounted afterburning turbojet engines.

The nacelles were suspended from the wing by bearing-mounted links which permitted the nacelles to translate freely in the axial direction. A load cell was installed

between the wing and the nacelle which measured the net longitudinal force of the nacelle. Details of airplane performance and flight characteristics due to aircraft modifications are presented in reference 1. Results from early research flights are reported in references 2 and 3. The primary objective of this program was to evaluate the installed efficiencies of various nozzle types for both supersonic cruise and supersonic dash aircraft. To do this, it was necessary to measure engine operating parameters accurately so that the internal thrust can be determined. The nozzle thrust minus drag also had to be determined.

The nozzle internal ideal thrust can be obtained by using the gas generator method (see ref. 4). In this method ground calibrations of the engine and afterburner are made, and inflight measurements of various temperatures and pressures are obtained and correlated with the calibrations to obtain the internal nozzle operating conditions. An alternate approach to determine nozzle internal gross thrust is to use a traversing rake at the nozzle exit. Results obtained by this method are reported in reference 5 for a turbojet engine and in reference 6 for a turbofan engine. In either case additional information is required regarding the flow field resulting from the interaction of the internal and external flows in evaluating the overall thrust and drag characteristics of a complete exhaust system. For simple exhaust system concepts it may be sufficient in determining nozzle drag just to measure the pressure force acting upon the exterior surfaces of the nozzle boattail. However, for more complex concepts (such as those utilizing auxiliary inlets) many more details of the flow influence the nozzle thrust minus drag propulsive force. The problem is further complicated when the external flow is distorted by the airframe installation effects. As a result it may not be practical to determine nozzle drag from pressure measurements since an excessive number of such measurements would be required.

The technique that was used in this program was to use the gas generator method to determine the nozzle ideal internal thrust (ref. 7). A load cell was used to measure the entire nacelle thrust minus drag, and the nozzle thrust minus drag was computed by subtracting all other drag forces acting on the nacelle (upstream of the nozzle) from the load cell force. The summation of these other drag forces was in effect the tare of the system. This tare had to be known for a range of mass flow ratios, engine power settings, and flight Mach numbers. The present report describes a series of flights that were used to evaluate nacelle tare forces using reference nozzles whose internal thrust had been ground calibrated (ref. 8) and whose external drag could be determined from simple pressure measurements on a base region. These tare forces were obtained over flight Mach numbers from 0.60 to 1.30, mass flow ratios from 0.70 to 0.97, and power settings from part power to maximum afterburning.

SYMBOLS

A	local cross-sectional area of nacelle, cm^2 ($in.^2$)
A_{max}	maximum cross section area of nacelle, 4230 cm^2 (657 $in.^2$)
A_8	primary nozzle exit effective flow area, cm^2 ($in.^2$)
a	nacelle axial acceleration, m/sec^2 (ft/sec^2)
C_F	ejector thrust coefficient, T/P_8A_8
C_f	skin friction drag coefficient
D	nozzle drag, N (lb)
D_{add}	inlet additive drag, N (lb)
D_b	base drag of ejector, N (lb)
D_{bump}	pressure drag on rearward-facing nacelle step, N (lb)
D_{cowl}	pressure drag and skin friction drag on inlet cowl, N (lb)
$D_{f_{nac}}$	skin friction drag on nacelle, N (lb)
D_{nac}	propulsion system drag force, N (lb)
D_{ram}	ram drag, mV_0, N (lb)
D_{strut}	pressure and skin friction drag on strut fairing, N (lb)
d	nacelle reference diameter, 63.50 cm (25.00 in.)
F_{lc}	force measured by load cell, N (lb)
g	force of gravity, m/sec^2 (ft/sec^2)
l	distance from wing chord line to top of strut fairing
M_0	flight Mach number
m	mass of air captured by inlet, mg (lb)
m_n	mass of nacelle, kg (slugs)
m_0	mass of air that could be captured by inlet if full-stream tube were swallowed; it is based upon free-stream density and velocity and inlet capture area having diameter of 37.37 cm (14.715 in.)
n	number of data points sampled
P_s	total pressure of secondary air, N/m^2 ($lb/in.^2$)
P_8	total pressure at primary nozzle, N/m^2 ($lb/in.^2$)

p_{I9}	internal static pressure at ejector exit, N/m^2 (lb/in.^{2} abs)
q	free-stream dynamic pressure, N/m^2 (lb/ft^2)
Re	Reynolds number
s	reference area, 2.21 m^2 (23.8 ft^2)
T	nozzle gross thrust, N (lb)
T_s	total temperature of secondary air, K (R)
t	wing thickness/2
V_0	free-stream velocity, m/sec (ft/sec)
w	strut thickness/2
x	distance on strut measured aft of strut fairing leading edge
x_n	distance on nacelle measured aft of inlet lip
x_w	distance along wing chord line measured aft from point of intersect of inlet lip plane and wing chord
y	distance from aircraft centerline to nacelle centerline
α_0	airplane angle of attack with respect to free stream, deg
δ	elevon deflection, deg
θ	nacelle angle with respect to earth horizontal, deg (rad)
σ	standard deviation
τ	ratio of secondary total temperature at exit of secondary passage to primary total temperature
ω	ratio of secondary to primary weight flow

APPARATUS

Installation

General location of the nacelle engine installations is shown in figure 1. Figure 2(a) is a detailed schematic of the aircraft showing the nacelle installation and aircraft dimensions. Each nacelle housed a J85-13 turbojet engine and afterburner. The nacelles were located 1.863 meters (73.34 in.) outboard of the airplane centerline at 34 percent semispan. The inlet lip was 3.498 meters (137.73 in.) aft of the wing leading edge. Shown in figure 2(a) is the reference nozzle installed on the right nacelle and a research nozzle

(variable flap ejector) installed on the left. Figure 2(a) also shows the portion of the elevon that was cut out to permit down elevon movement on each side of the nacelle (ref. 6).

The nacelle installation is shown in figure 2(b). The nacelle was inclined 4.5° down with respect to the wing chord line to make the aft portion of the nacelle tangent to the lower surface of the wing at its trailing edge.

The strut fairing is shown in figure 3(a). A gap of 0.64 centimeter (0.25 in.) was maintained between the lower wing surface and the strut fairings. These struts were mounted directly to the nacelle.

Details of the elevon cutout and fixed portion of the elevon are shown in figure 3(b). Approximately 18 percent of the elevon surface was removed for this modification.

A schematic drawing of the nacelle is presented in figure 4. The exhaust nozzle was considered to be that portion located downstream of the nozzle reference plane (station 127.68). The flat-bottomed bulge on the nacelle shown in sections A-A and B-B was necessitated by the J-85 engine accessory package.

The area distribution of the nacelle with and without the strut fairing is shown in figure 5. The maximum area occurs at the location of the bulge where the area is 4230 square centimeters (657 in.^{2}). At this station the strut fairing added 5 percent to the basic nacelle area.

Details of the rounded inlet cowl lip are shown on figure 6. The inlet capture area was based upon the 37.336-centimeter (14.715-in.) diameter. Secondary air to the nozzle was supplied through a conical rotating valve shown in the sketch of the inlet (fig. 7). The valve calibrations were done in the Propulsion System Laboratory at the Lewis Research Center in conjunction with the reference nozzle calibrations. Metered flow was introduced into a manifold upstream of the compressor face and was directed through an annular channel to the valve (fig. 8).

These valve calibrations were refined during the flight program by using the reference nozzle pumping characteristics which had been determined during their ground calibrations. This refinement for the flight test data was presumably necessary because of differences in the velocity profiles within the inlet ahead of the valve as compared to those in the calibration manifold. Secondary flow rates computed from the reference nozzle pumping characteristics were used to establish an effective flow coefficient for the valve. Figure 9 shows details of the reference nozzles. Two different nozzle sizes were used, and the dashed lines shows the contour of the smallest nozzle. The ejector shroud was cylindrical so that pressure forces would provide no axial force except that acting on the annular base cavity. The secondary flow deflector was necessary to direct secondary flow through 24 holes in the nozzle housing ring to assure cooling airflow over the primary nozzle leaves. The reference nozzles were instrumented as shown in figure 10. The static pressures at the nozzle exit station were used to correlate nozzle internal per-

formance with previous calibrations. Selected temperatures on the nozzle were monitored in flight to preclude exceeding temperature limits.

Thrust Measurement System

The nacelle support system, shown in figure 11, consisted of a front link, a rear link, and a thrust sensor assembly located between the two links. The front and rear links were each attached to a wing fitting and a nacelle fitting with ball bearings. Each link was installed so that a line through the axis of rotation of the upper and lower bearings was perpendicular to the nacelle thrust axis. The front and rear links transferred all loads acting on the nacelle directly to the wing except loads acting in the direction of the nacelle thrust axis. These loads were transferred to the wing through the load cell whose axis was parallel to that of the nacelle.

The load cell was a miniature type containing a semiconductor strain-gage bridge and was vented so that no cell tare force was encountered due to pressure variations. It was attached to a nacelle fitting and a wing fitting through spherical bushings and was installed so that a line through the axis of rotation of the two bushings was approximately parallel to the nacelle thrust axis.

The load cell measured the net longitudinal force between the nacelle and the wing as shown by the following equation:

$$F_{lc} = T - D_{nac} - m_n(a + g \sin \theta) \tag{1}$$

A signal proportional to the acceleration term $(a + g \sin \theta)$ was obtained from a servoaccelerometer mounted in the nacelle. This accelerometer contained a high gain amplifier circuit which electrically balanced the acceleration forces on a flexure-suspended seismic mass. The acceleration-sensitive axis of this unit was alined parallel to the nacelle centerline.

The method by which the load cell and accelerometer signals were combined is shown schematically in figure 12. The setting of this potentiometer determined the portion of the servoaccelerometer signal which was subtracted from the load cell signal to obtain the net thrust minus drag output (load cell compensated reading). The potentiometer was adjusted on the ground to give a zero output since the output should be zero at static conditions. Low pass filters were incorporated in both the load cell and accelerometer circuits to attenuate frequencies higher than the natural frequency of the nacelle support system (23 Hz). The load cell compensated reading was recorded 48 times during a data scan.

To maintain a constant temperature environment, the accelerometer mounting block

and both ends of the load cell were equipped with heaters and thermoswitches, and the accelerometer and load cell were wrapped with insulation. The temperature of these units was maintained within 11 K (20° R) of 311 K (560° R).

In ground calibrations, the accuracy of the load cell reading compared with known forces applied to the nacelle was within ±0.1 percent of full scale. This included hysteresis, nonlinearity, and data recording system errors, but did not include errors due to changes in temperature or acceleration compensation. The overall system accuracy is estimated as ±0.25 percent of full scale.

Airborne Data Acquisition System

The data system was designed to achieve an inherently high accuracy and repeatability. Wherever possible, the transducers, instruments, and techniques used were those which had proven to give consistently accurate results with good reliability in other programs. Also incorporated in this program was the preselection of transducers to obtain the best units of a type, and thermostatically controlled electrical heating of the transducers was used to minimize thermal drift during the flight.

The data acquisition system, as shown in figure 13, consisted of a system to multiplex and record quasistatic data in digital form on magnetic tape, and a system to record dynamic data and variations in flight parameters in FM analog form on a second magnetic tape. A transducer signal patchboard was used to select the signals of interest in a particular flight for each recording system. Major components of the data system are illustrated in figure 14.

Static steady-state pressures were sampled by means of Scanivalves. The Scanivalve unit contained a solenoid-actuated rotating pressure passage which sequentially connected 48 pressure lines to a single transducer. Ten Scanivalves, located in the two nacelles, provided for a capacity of 480 pressure measurements.

Each of the pressures was recorded only once during a data scan. Thermocouples, potentiometers and other transducer outputs were sampled and recorded six times during a scan. The total scan of 11.52 seconds included 1152 words. The details of sequencing of a data scan are given here.

The digital data recording system utilized a multiplex system (fig. 15) which sequentially sampled three groups of differential input signals. The 12 type A inputs were signals from 10 Scanivalve pressure transducers (A1 to A10), and two load cells (A11 and A12). The 48 type B inputs and 48 type C inputs were signals from thermocouples, potentiometers, and various other transducers.

During a data scan, these three groups of signals were sampled by the multiplexer at a rate of 100 per second. The scanning sequence followed a pattern of frames, as illustrated in figure 16, in which each of the 10 Scanivalves were read (A inputs) every 24 data

input readings, and the type B and C inputs were repeated every 192 readings (eight frames).

At the start of a data scan, the 10 Scanivalves were positioned at the home pressure port (Port 48). During the first frame, input A1 (Scanivalve 1, Port 48) was read, then B1 (first input in B group), then A2 (Scanivalve 2, Port 48), then C1 (first input in C group), and so forth through B6, A12, and C6. After each group of two Scanivalves were read, a command to step to the next port was given. During Frame 2, the next port (Port 1) on each Scanivalve and the following six inputs on the B and C groups were read. At the end of eight frames, all 48 inputs on the B and C groups had been read, and sampling of these groups for the second time was begun on the ninth frame. The data scan was completed at the end of 48 frames, and contained six samples each of the B and C inputs, one sample of each of the 480 Scanivalve ports, and 48 samples each of the two thrust readings on A11 and A12.

After amplification and zero-shifting, the analog signal samples from the multiplexer were each converted to a 120-bit binary word. This word was recorded in a computer-compatible format on a seven-track incremental tape recorder. Each data word consisted of two characters, each character consisting of six data bits and an odd parity bit. In addition to the data words, general information such as date, time, flight number, program number, and reading number were recorded before each data scan.

The maximum error specification for the digital data system required that 99.73 percent of the samples (three sigma, with a normal distribution) would be within ±0.34 percent of full scale. This included errors from all sources (ambient temperature and pressure, nonlinearity, gain inaccuracy, zero offset, drift, noise, etc.) except the transducers. To check this accuracy, a reference voltage was recorded by the data system during each scan. The maximum error of this reading from data recording during research flights was within ±0.1 percent of full scale.

Dynamic data were recorded on a 14-track analog tape recorder. The pilot's voice was recorded on an edge track. Either FM or direct record amplifiers could be used for any channel. At a tape speed of 38.1 centimeters per second (15 in./sec), the frequency response of the FM channels was dc to 5 kilohertz, and that of the direct channels was 300 to 62.5 kilohertz. Although data were taken, none are presented herein.

Each tape track could be utilized for six data inputs with the use of proportional bandwidth multiplex units. The frequency response of the 48 multiplex units in the system was dc to 400 hertz.

A telemetry link to a ground-based control room was used for observation of critical aircraft parameters. Nine proportional bandwidth channels were provided which varied in upper frequency limit from 11 to 160 hertz. Telemetry was used during flutter flights to clear the modified airplane throughout the test profile.

METHOD OF THRUST MEASUREMENT

The primary objective of this series of flights was to determine the repeatability of the system in calculating performance of exhaust nozzles. This was done using reference ejector nozzles having known thrust performance. Secondary weight flow to the nozzles was varied so that the effect of changes in inlet capture mass flow could be evaluated.

Flights were flown over the Mach number range of 0.6 to 1.3 along the profile shown in figure 17. This profile was chosen to minimize elevon trim excursions, angle-of-attack variations, and to operate near the full-scale range of the pressure transducers. Angle of attack and elevon deflections along this profile are shown in figure 18.

Calibration flights were made several times during the program. This was done to check the repeatability of the system and to obtain additional data as the need arose.

Data for Mach numbers 0.60 and 0.70 were obtained with the reference nozzle with a smaller exit area diameter (34.5 cm or 13.60 in.). This smaller area allowed the primary flow to be attached within the ejector shroud whereas it was detached at the same pressure ratios for the large nozzle. This attached flow condition provided a high degree of confidence in using the prior ground calibrations of the internal nozzle thrust.

In evaluating performance of various research nozzles the nozzle thrust minus drag is usually ratioed to the ideal thrust of the primary jet. The primary thrust is obtained from the engine calibrations of reference 7, utilizing the gas generator method. The nacelle thrust and drag forces are shown in figure 19. All axial forces downstream of station 127.68 are assigned to the nozzle and all forces upstream are assigned to the nacelle. The research nozzle thrust minus drag is given by the following equation:

$$T - D = \text{Tare} + \left[F_{lc} + m_n(a + g \sin \theta)\right] \tag{2}$$

Tare is defined as the summation of nacelle drag forces; that is,

$$\text{Tare} = D_{ram} + D_{add} + D_{bump} + D_{cowl} + D_{nac} + D_{strut} \tag{3}$$

In order to use equation (2) to evaluate research nozzle performance, the Tare force must be obtained. This was done in the present investigation by using the calibrated reference nozzle. Reference nozzles were installed on both nacelles. The exit conditions at the primary nozzle were determined by using the gas generator method for engines calibrated for airflow, afterburner pressure drop, and afterburner temperature rise characteristics. The internal thrust of each reference nozzle was determined by correlation of a nozzle thrust coefficient C_F with the nozzle operating conditions. The nozzle had been

ground calibrated where C_F was determined as a function of the ratio of internal ejector static pressure to primary nozzle pressure p_{I9}/P_8 corrected secondary flow $\omega\sqrt{\tau}$ and primary area A_8. The external drag of each reference nozzle was found by pressure measurement in the known base area and by calculation of a skin friction drag. Skin friction was calculated using flat plate theory with the friction coefficient defined as $C_f = 0.075/Re^{1/5}$. The bracketed term in equation (2) is the compensated load cell reading. The difference between the reference nozzle thrust minus drag T - D and the compensated load cell force is the nacelle tare force.

RESULTS

Evaluation of Tare Forces

Tare forces were calculated over the range of Mach number, mass flow ratio, and engine power setting. These tare forces presented as coefficients are shown in figure 20. It was not practical to obtain data points at the discrete Mach numbers shown. The raw data were within approximately 0.02 of the Mach numbers shown and were adjusted for this small deviation using the measured variation of tare with Mach number. It was suspected that there might be a difference in tare force from left to right nacelles at the same mass flow ratio due to misalinements or geometric differences due to tolerances, and so forth. However, the data showed no consistent differences between left and right sides. It was also expected that the tare coefficients would vary with mass flow because ram drag, additive drag, and cowl pressure drag are strong functions of mass flow ratio. Therefore, secondary flow was varied from corrected values of 0.02 to 0.08 to obtain data over the desired range.

The tare coefficients were found to vary nearly linearly with mass flow ratio for all Mach numbers. An initial least squares linear curve fit was made of all military power data for both left and right nacelles at each Mach number. Crossplots of the data of figure 20 were then made at a mass flow ratio of 0.82 as a function of Mach number and are presented in figure 21. The curve of figure 21 was used to adjust the data points of figure 20 for deviation in Mach number by using the slope at each Mach number. The nacelle tare force is most sensitive to flight Mach number in the region from Mach 0.9 to 1.0.

To obtain the nacelle tare needed in equation (2) values of tare are read from figure 21. Tare coefficients are adjusted for variation in inlet mass flow ratio from the value of 0.82 of figure 21 by the following equation:

$$\frac{\text{Tare}}{qs} = \left(\frac{\text{Tare}}{qs}\right)_{m/m_0 = 0.82} + \frac{\frac{d(\text{Tare})}{qs}}{d\left(\frac{m}{m_0}\right)}\left[\left(\frac{m}{m_0}\right)_{\text{desired}} - 0.820\right] \tag{4}$$

The slope of Tare as a function of m/m_0 is obtained from figure 22. These slopes were obtained from figure 20. The contribution of ram drag to the slope is also shown on the figure. The nacelle tare force is most sensitive to change in inlet mass flow ratio between Mach 0.60 and 0.70 (fig. 22).

As can be seen on figures 20(c), (e), and (g), the scatter of data or deviation from the curve becomes greater when the engine is afterburning. Only the left engine afterburning data are presented, but the right engine data exhibit the same tendency. The afterburner data not only show random deviation but are also biased. That is, all the minimum reheat data lie lower than military data and the maximum reheat data lie above the military.

These apparent biases in afterburning are thought to be the result of biases in the determination of reference nozzle thrust coefficients during calibration and possible inaccuracies in the engine afterburner calibrations. The tare coefficient in maximum afterburning is very sensitive to inaccuracies in the reference nozzle thrust coefficient because the thrust level is higher. A 1-percent inaccuracy in thrust coefficient at maximum afterburning produces a 3.64-percent error in tare coefficient.

No account is made for these biases and the true tare is taken to be that calculated from military data only. All the curves of figure 20 were established using only military data.

Another aspect of the tare force evaluations was that the tare force on one nacelle was not affected by power settings on the opposite nacelle. This fact was determined by maintaining military power on one nacelle and varying power on the opposite engine. No change in tare was experienced at any power setting. This is shown on figure 20(e) where the tare coefficient on the right nacelle does not change when power is varied on the left side. Point (a) was the right tare coefficient with maximum reheat on the left nacelle, point (b) with military on left, and point (c) with minimum reheat on the left.

Statistical Results

An estimate was made of the random error in determining nacelle tare forces or the repeatability of the system. A computer computation was made of the standard deviation of all military power data points (left and right) from the data of figure 20. This calculation was made at each discrete Mach number. The results are presented in figure 23.

The standard deviation of the data is defined as follows:

$$\sigma = \sqrt{\frac{\sum y_i^2}{n}}$$

where

σ standard deviation

y_i difference in tare coefficient between data point and curve

n number of data points

Figure 23 shows the standard deviation as a percent of tare as a function of Mach number. Also shown is the level of error in tare necessary to yield a 1-percent error in T - D. The standard deviation of all the data is shown to be within ±1 percent error in thrust minus drag.

The standard deviation of the data for afterburning on the left side was also calculated. These results are shown in figure 24. These data points show larger deviations than military data alone. From Mach 0.80 to 1.06 the one sigma deviation would produce slightly less than 2 percent error in thrust minus drag. This comparison includes the possible errors in determining reference nozzle afterburning thrust coefficients.

These errors are not present when research data are taken so that the error in measuring thrust minus drag of research nozzles should exhibit accuracies less than those shown in the figure. No afterburning data were taken below Mach 0.80. Therefore the curves do not extend below this Mach number on figure 24.

The probability distribution of all military power data (340 points) was compared to that of a normal distribution with a mean tare coefficient error of -1.00×10^{-4} and a standard deviation of 20.45×10^{-4}. This is the mean and standard deviation calculated from the data. If the data were perfectly curve fit by a least squares method the mean error would be zero. However, the curves used were the average of the curve fits of the left and right nacelles. A plot of these distributions is shown in figure 25. The sample distribution has a greater concentration of data in the region of low random error than the normal distribution. The sample has 72 percent of the data less than one sigma whereas the normal distribution includes 68 percent of the data less than one sigma.

SUMMARY OF RESULTS

Flight tests were conducted on a modified F-106 aircraft having thrust measuring systems on two underwing nacelles containing J85-13 turbojet engines. The program was conducted using reference nozzles having known thrust performance to determine the nacelle tare forces in the system. The effects of Mach number, mass flow ratio, and engine power settings were determined. The following results were obtained:

1. Tare forces were obtained as a function of Mach number whose random errors were nearly Gaussian and which resulted in a repeatability of ±1.0 percent in the calculation of nozzle performance for 68 percent of the data.

2. No appreciable cross flow effects of one nacelle installation on the other were observed.

3. No appreciable difference in nacelle tare force between the left and right nacelles was observed.

Lewis Research Center,
National Aeronautics and Space Administration,
Cleveland, Ohio, May 26, 1971,
720-03.

REFERENCES

1. Crabs, Clifford C.; Mikkelson, Daniel C.; and Boyer, Earle O.: An Inflight Investigation of Airframe Effects on Propulsion System Performance at Transonic Speeds. Presented at the 13th Annual Symposium of the Society of Experimental Test Pilots, Los Angeles, Calif., Sept. 25-27, 1969.

2. Mikkelson, Daniel C.; and Head, Verlon L.: Flight Investigation of Airframe Installation Effects on a Variable Flap Ejector Nozzle of an Underwing Engine Nacelle at Mach Numbers from 0.5 to 1.3. NASA TM X-2010, 1970.

3. Wilcox, Fred A.; Samanich, Nick E.; and Blaha, Bernard J.: Flight and Wind Tunnel Investigation of Installation Effects on Supersonic Cruise Exhaust Nozzles at Transonic Speeds. Paper 69-427, AIAA, June 1969.

4. Beaulieu, Warren; Campbell, Ralph; and Burcham, William: Measurement of XB-70 Propulsion Performance Incorporating The Gas Generator Method. J. Aircraft, vol. 6, no. 4, July-Aug. 1969, pp. 312-317.

5. Davidson, Theron W.: Method of Net Thrust Measurement in Supersonic Flight. Aerodynamics of Power Plant Installation, Part I. Agardograph 103, pt. 1, Oct. 1965, pp. 217-243.

6. Waters, M. H.; and Graham, P. A.: Evaluation of an Exhaust Nozzle Traversing Rake System as an In-Flight Thrust Measuring Device for an Afterburning Turbofan Engine. Rep. NAPTC-ATD-150, Naval Air Propulsion Test Center, Nov. 1968.

7. Antl, Robert J.; and Burley, Richard R.: Steady-State Airflow and Afterburning Performance Characteristics of Four J86-GE-13 Turbojet Engines. NASA TM X-1742, 1969.

8. Samanich, Nick E.; and Huntley, Sidney C.: Thrust and Pumping Characteristics of Cylindrical Ejectors Using Afterburning Turbojet Gas Generator. NASA TM X-52565, 1969.

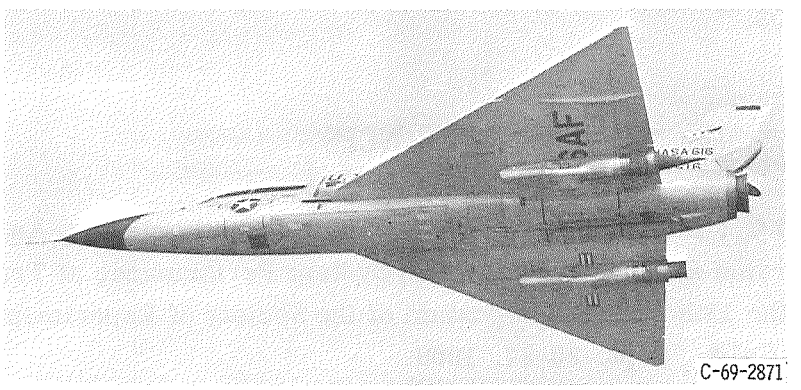

Figure 1. - Modified F-106 aircraft.

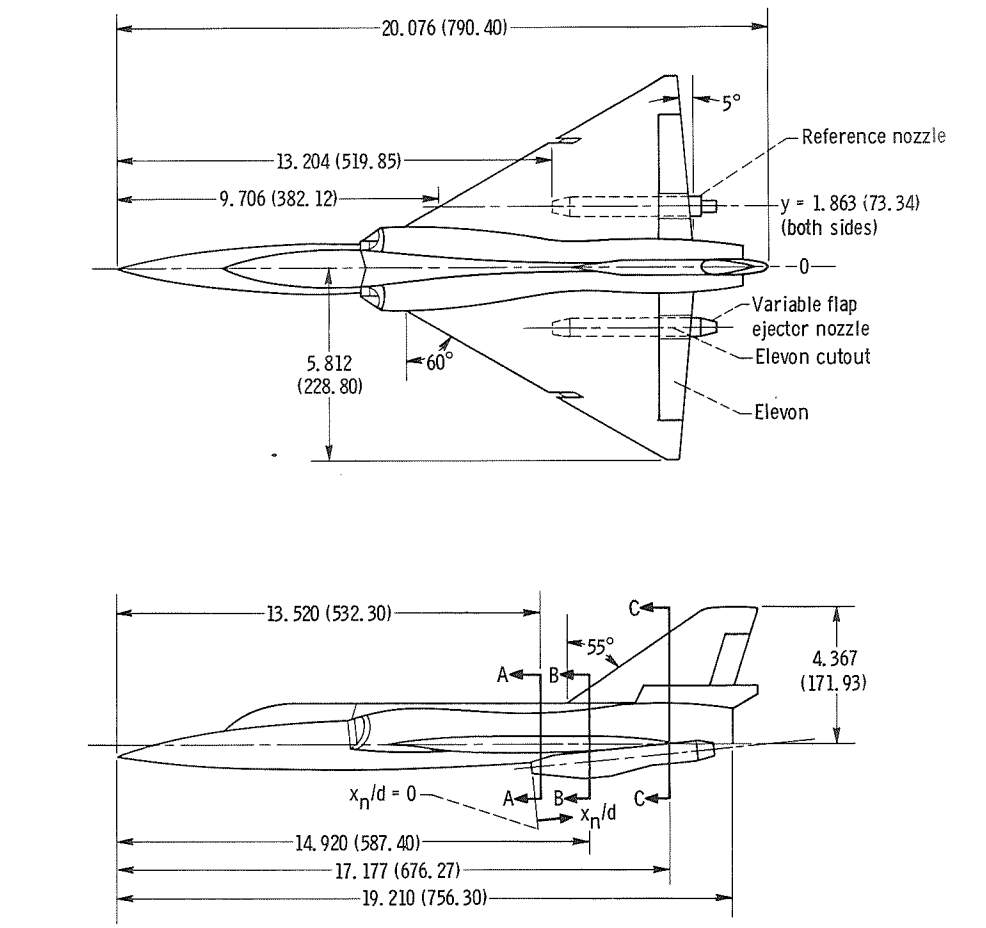

(a) Aircraft details.

Figure 2. - Aircraft details and installation of nacelles under the wing.
(All dimensions in m (in.) unless indicated otherwise.)

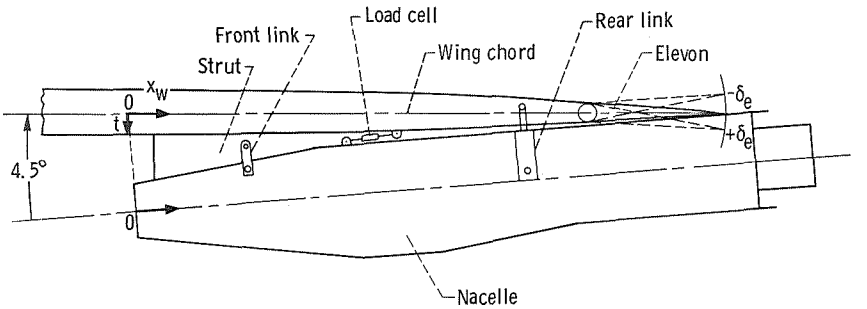

Wing lower-surface coordinates (d = 63.50 cm or 25.00 in.)			
x_w/d	t/d	x_w/d	t/d
0	0.225	3.613	0.166
.338	.226	4.202	.145
1.069	.225	4.754	.107
2.282	.218	5.402	.062
2.802	.196	6.257	.004

(b) Nacelle installation.

Figure 2. - Concluded.

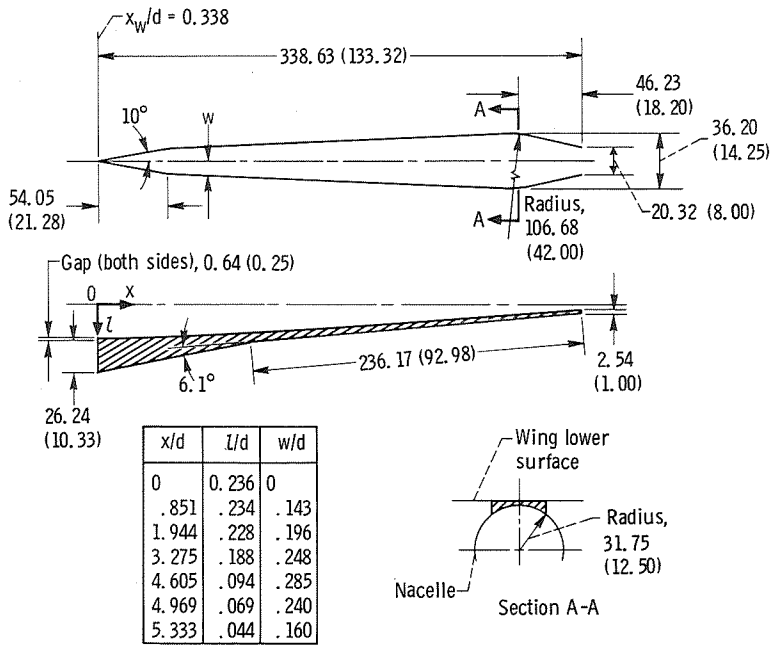

x/d	l/d	w/d
0	0.236	0
.851	.234	.143
1.944	.228	.196
3.275	.188	.248
4.605	.094	.285
4.969	.069	.240
5.333	.044	.160

(a) Wide nacelle strut fairing.

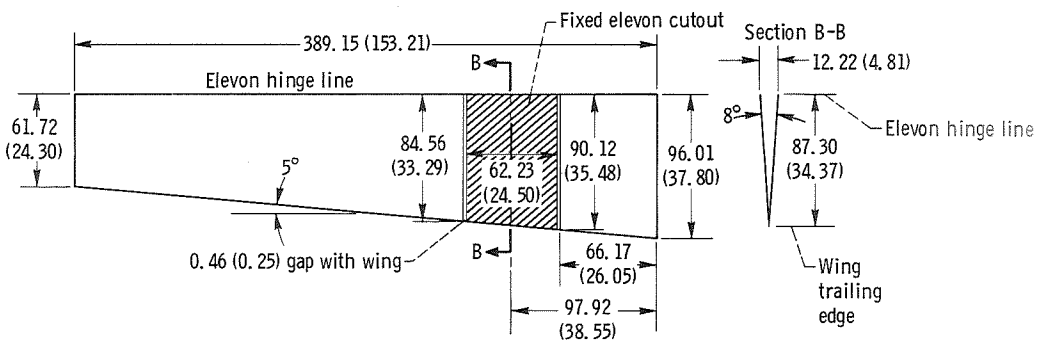

Section B-B

	x_w/d	x_n/d
Elevon hinge line	4.912	4.945
Wing trailing edge	6.290	6.240

(b) Elevon.

Figure 3. - Nacelle strut fairings and elevon. (All dimensions in cm (in.) unless indicated otherwise.)

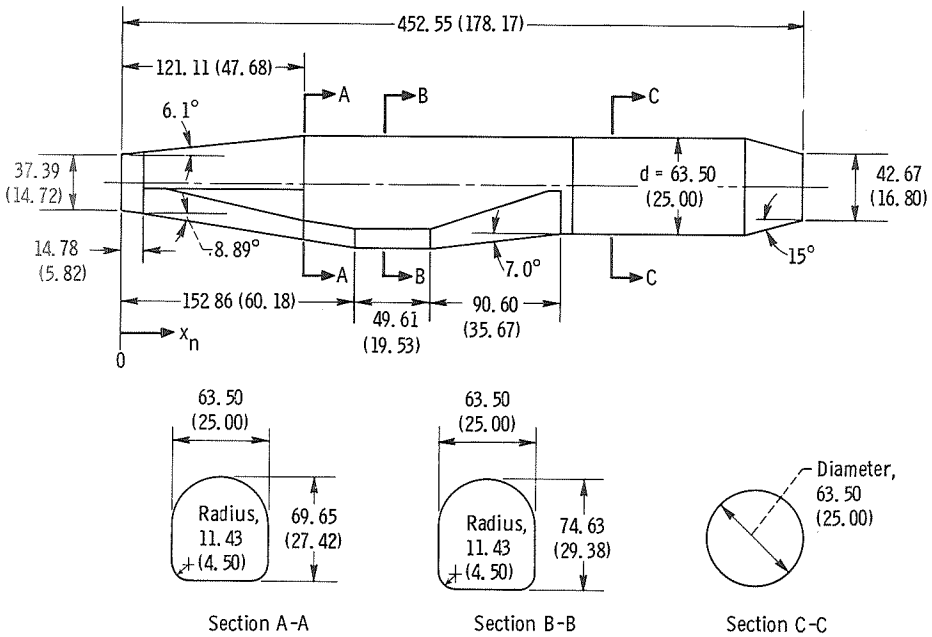

Figure 4. - Nacelle. (All dimensions in cm (in.) unless indicated otherwise.)

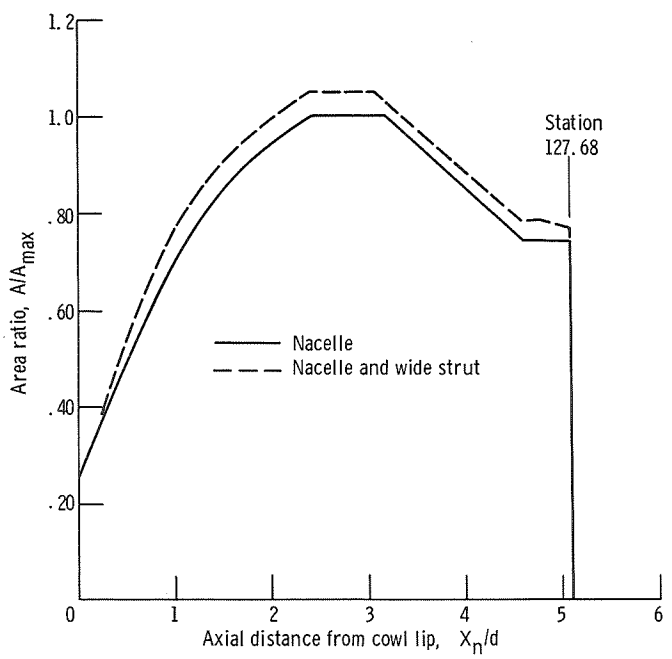

Figure 5. - Nacelle cross-sectional area distribution. Maximum cross section area of nacelle A_{max} = 4230 square centimeters (657 in.^{2}).

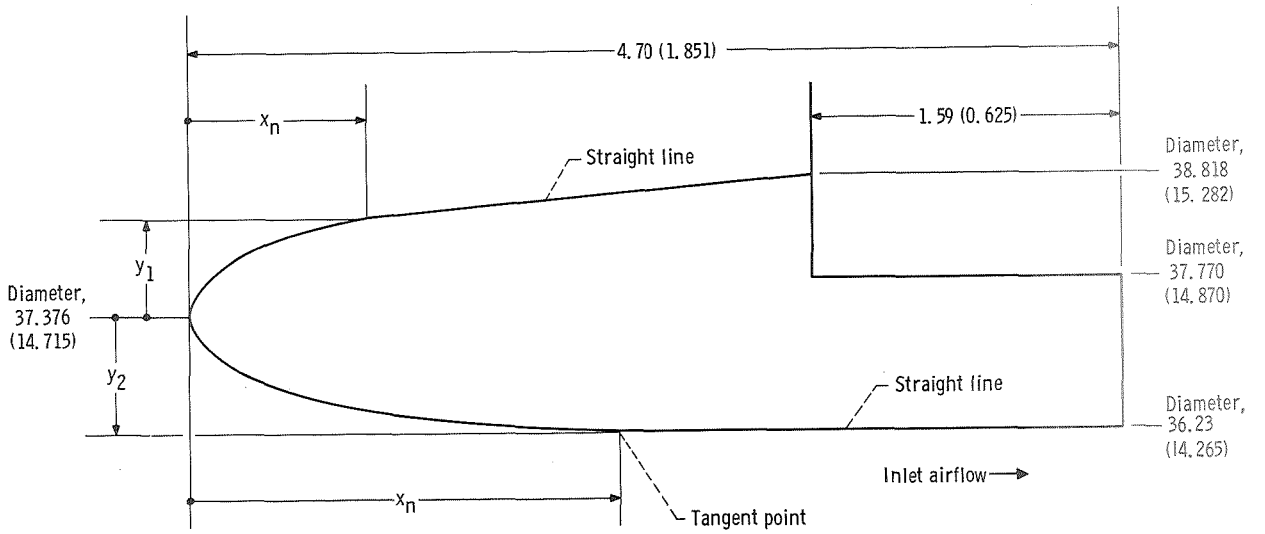

x_n		y_1		y_2	
cm	in.	cm	in.	cm	in.
0.000	0.000	0.000	0.000	0.000	0.000
.053	.021	.135	.053	.135	.053
.129	.051	.328	.083	.328	.083
.231	.091	.277	.109	.277	.109
.383	.151	.973	.138	.973	.138
.637	.251	.437	.172	.437	.172
.891	.351	.500	.197	.500	.197
1.145	.451	----	----	.546	.215
1.399	.551	----	----	.579	.228
1.653	.651	----	----	.599	.236
1.907	.751	----	----	.612	.241
2.161	.851	----	----	.617	.243

Figure 6. - Cowl lip contour. (All dimensions in cm (in.).)

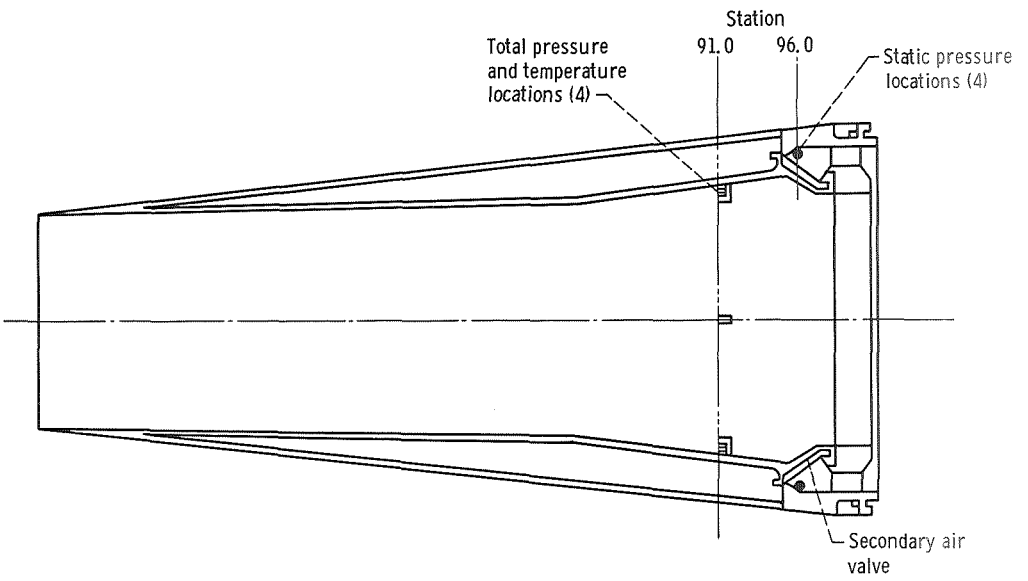

Figure 7. - Instrumentation of flight inlet.

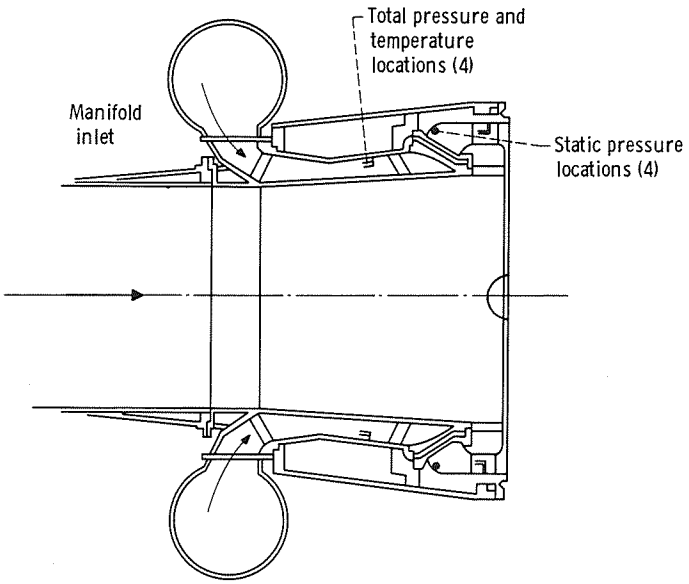

Figure 8. - Secondary flow calibration manifold.

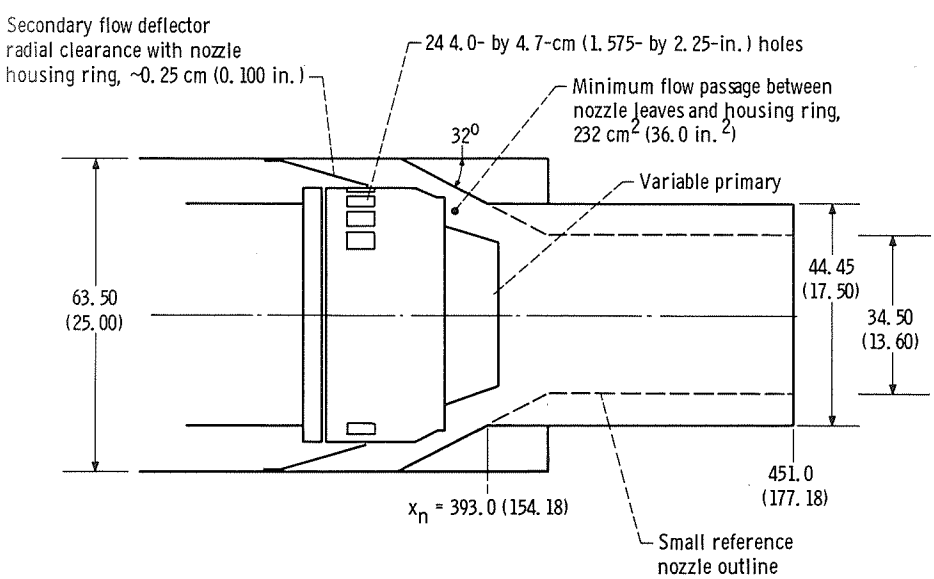

Figure 9. - Details of reference nozzles. (All dimensions in cm (in.) unless indicated otherwise.)

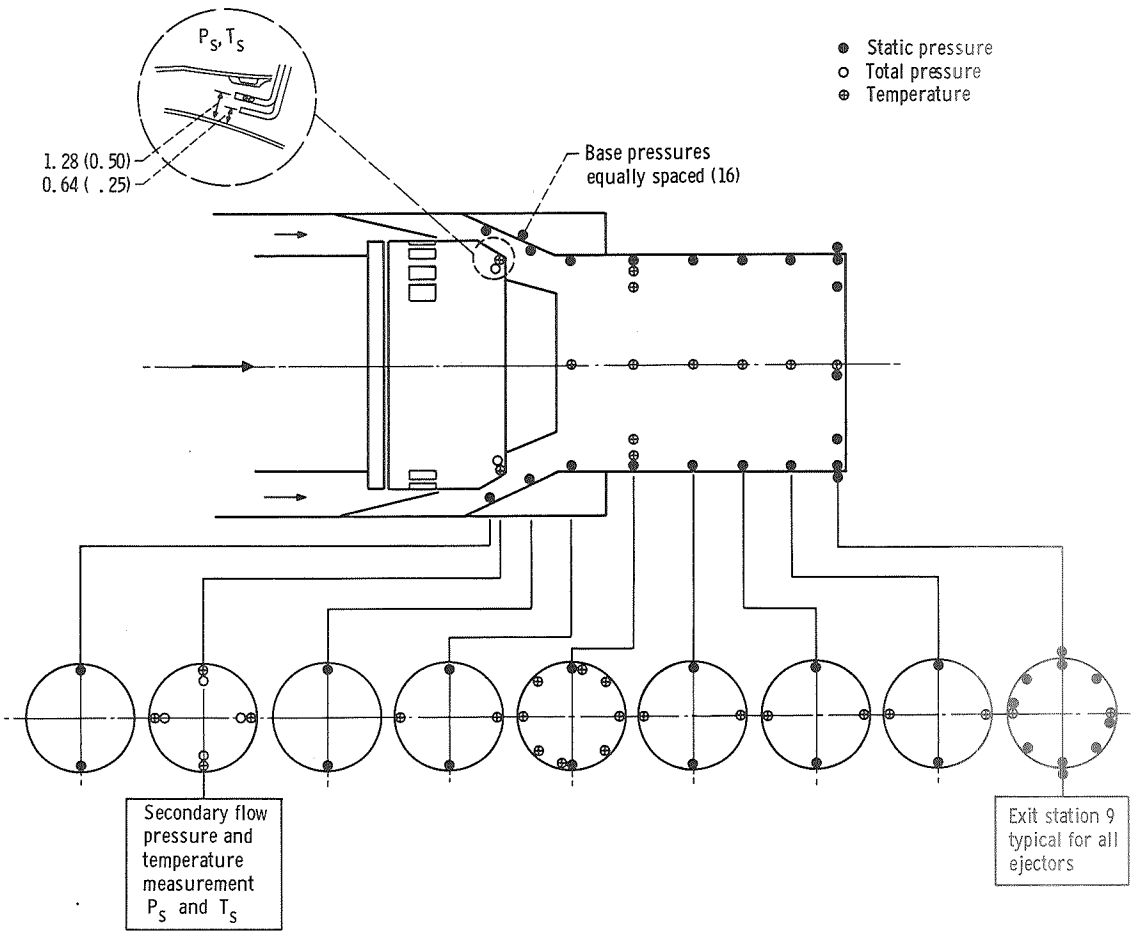

Figure 10. - Instrumentation details of reference nozzle. (All dimensions in cm (in.) unless indicated otherwise.)

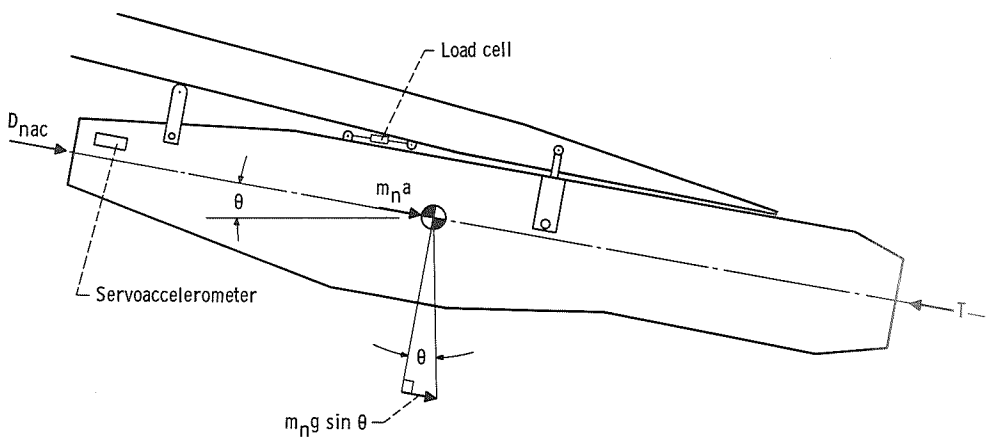

Figure 11. - Nacelle force diagram.

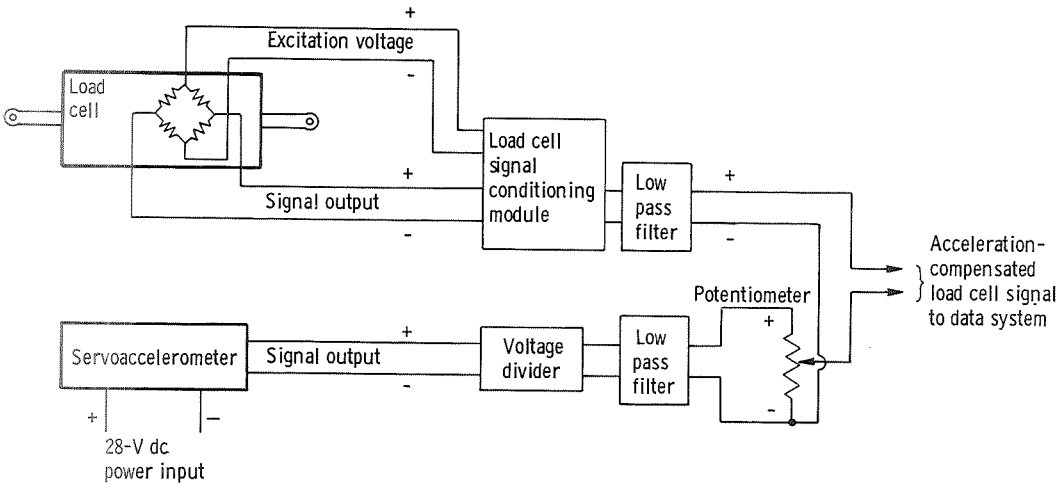

Figure 12. - Load cell compensation.

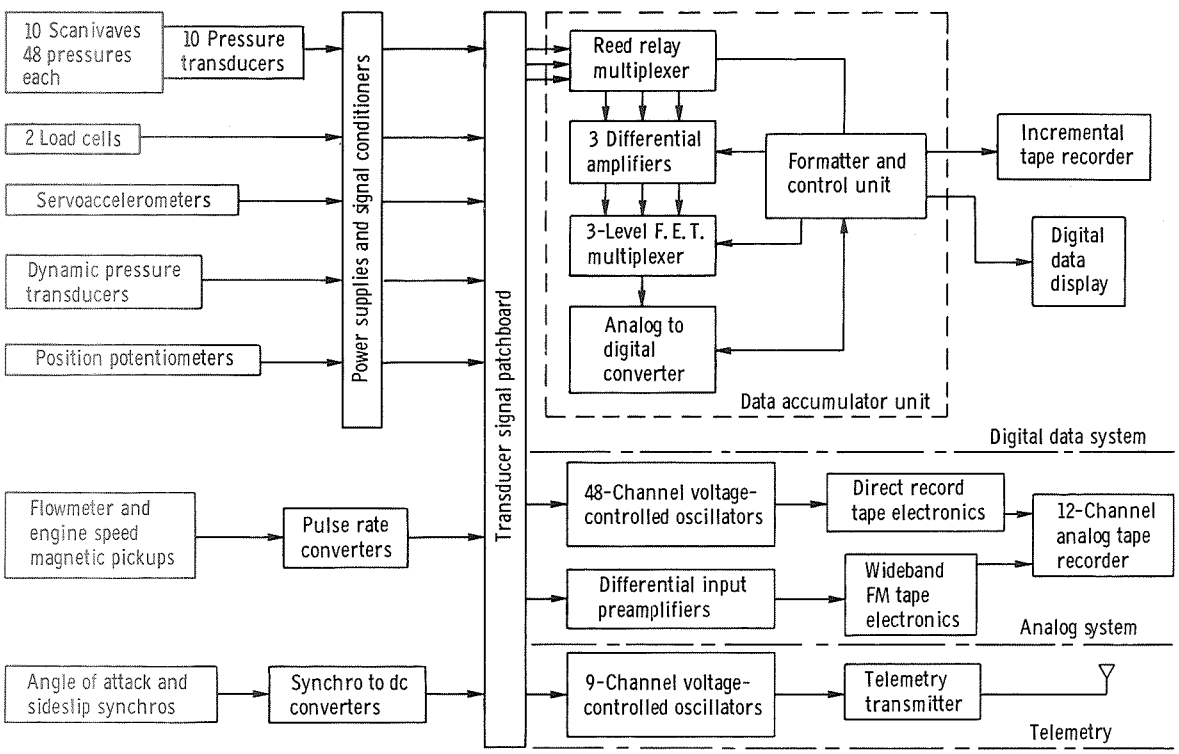

Figure 13. - Data acquisition system schematic.

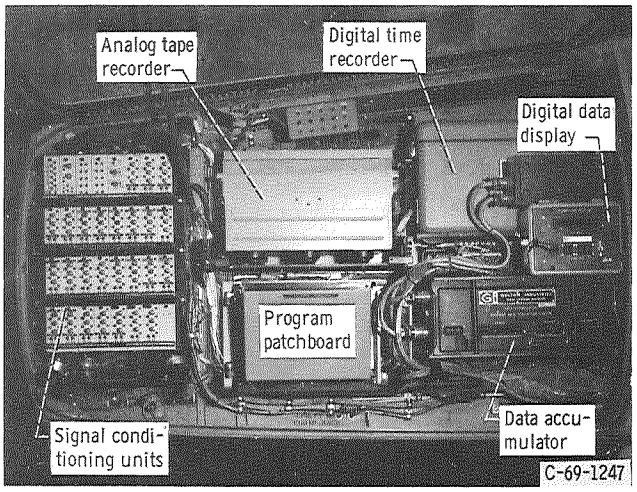

(a) Left forward electronics compartment (nose).

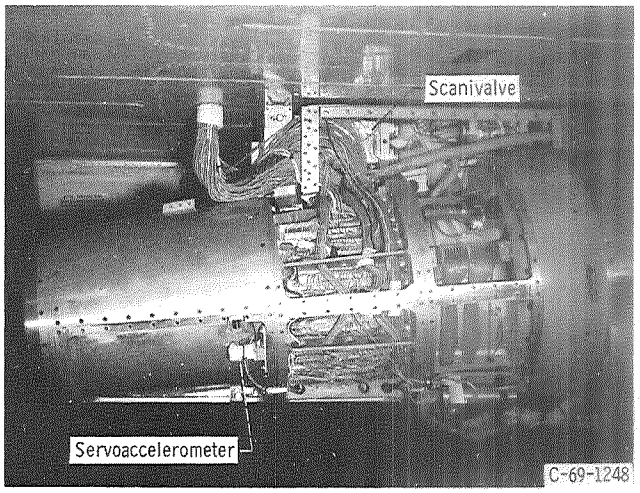

(b) Left nacelle inlet with cover panels removed.

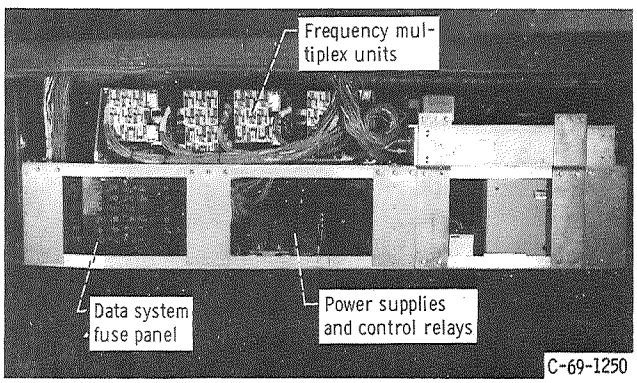

(c) Right side missile bay rack, lowered.

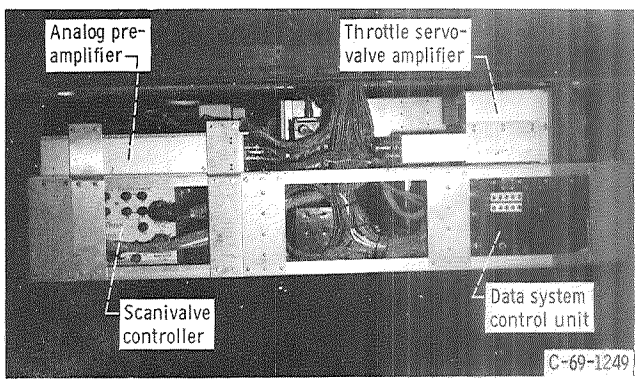

(d) Left side missile bay rack, lowered.

Figure 14. - Data acquisition system components.

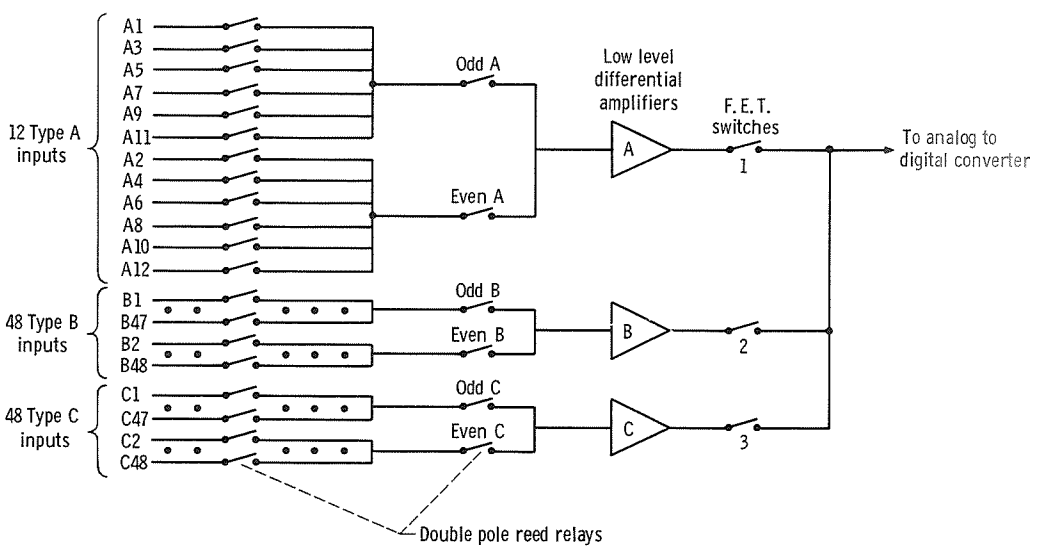

Figure 15. - Multiplexer schematic.

General information words

Frame 1			Frame 2			Frame 8			Frame 48		
Data word reading number	Relay number	Step Scanivalve	Data word reading number	Relay number	Step Scanivalve	Data word reading number	Relay number	Step Scanivalve	Data word reading number	Relay number	Step Scanivalve
1	A1	1 and 2	25	A1	1 and 2	169	A1	1 and 2	1129	A1	1 and 2
2	B1		26	B7		170	B43		1130	B43	
3	A2		27	A2		171	A2		1131	A2	
4	C1		28	C7		172	C43		1132	C43	
5	A3	3 and 4	29	A3	3 and 4	173	A3	3 and 4	1133	A3	3 and 4
6	B2		30	B8		174	B44		1134	B44	
7	A4		31	A4		175	A4		1135	A4	
8	C2		32	C8		176	C44		1136	C44	
9	A5	5 and 6	33	A5	5 and 6	177	A5	5 and 6	1137	A5	5 and 6
10	B3		34	B9		178	B45		1138	B45	
11	A6		35	A6		179	A6		1139	A6	
12	C3		36	C9		180	C45		1140	C45	
13	A7	7 and 8	37	A7	7 and 8	181	A7	7 and 8	1141	A7	7 and 8
14	B4		38	B10		182	B46		1142	B46	
15	A8		39	A8		183	A8		1143	A8	
16	C4		40	C10		184	C46		1144	C46	
17	A9	9 and 10	41	A9	9 and 10	185	A9	9 and 10	1145	A9	9 and 10
18	B5		42	B11		186	B47		1146	B47	
19	A10		43	A10		187	A10		1147	A10	
20	C5		44	C11		188	C47		1148	C47	
21	A11		45	A11		189	A11		1149	A11	
22	B6		46	B12		190	B48		1150	B48	
23	A12		47	A12		191	A12		1151	A12	
24	C6		48	C12		192	C48		1152	C48	

Generate end of record gap

Figure 16. - Multiplexer scanning sequence.

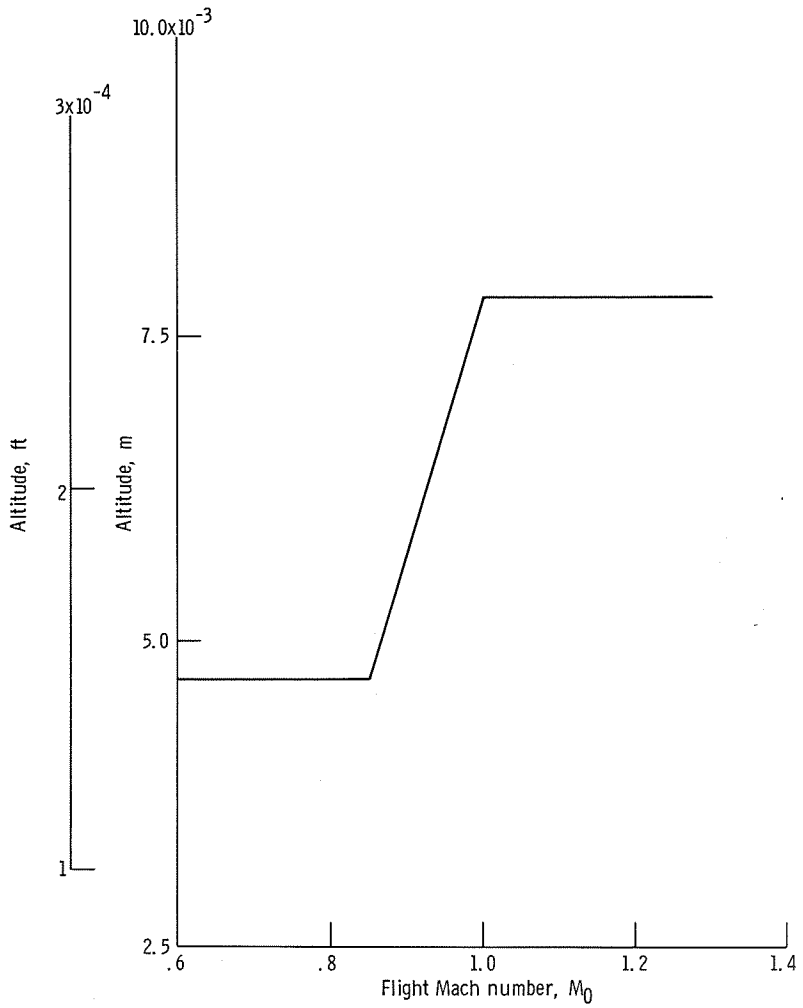

Figure 17. - Flight profile.

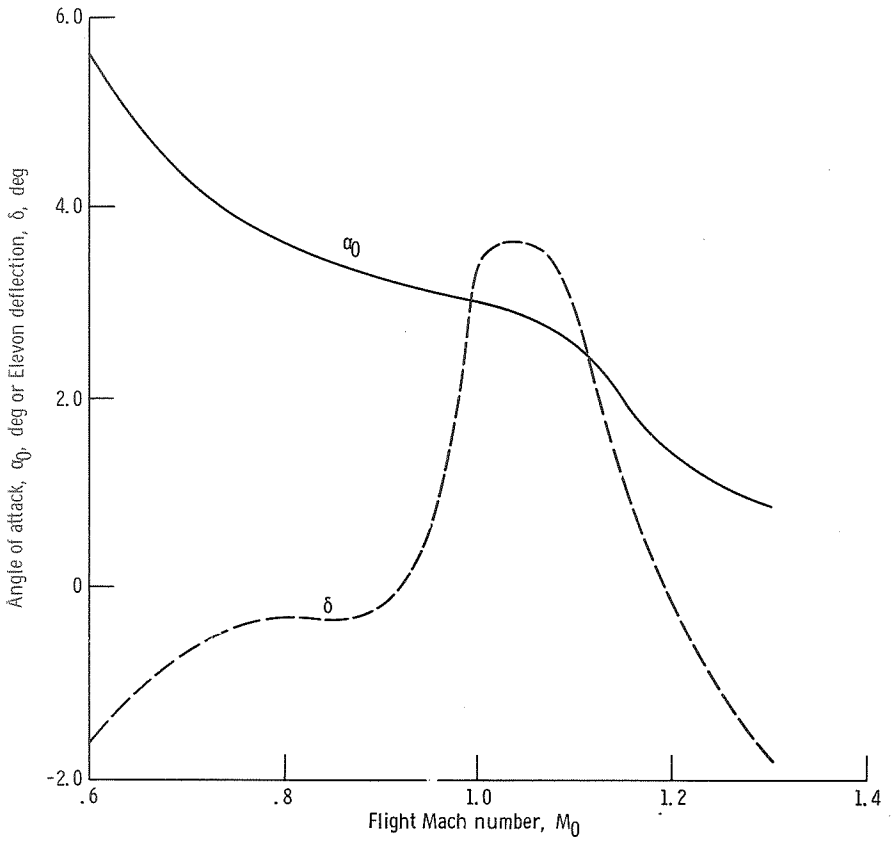

Figure 18. - Angle of attack and elevon deflection over flight test profile.

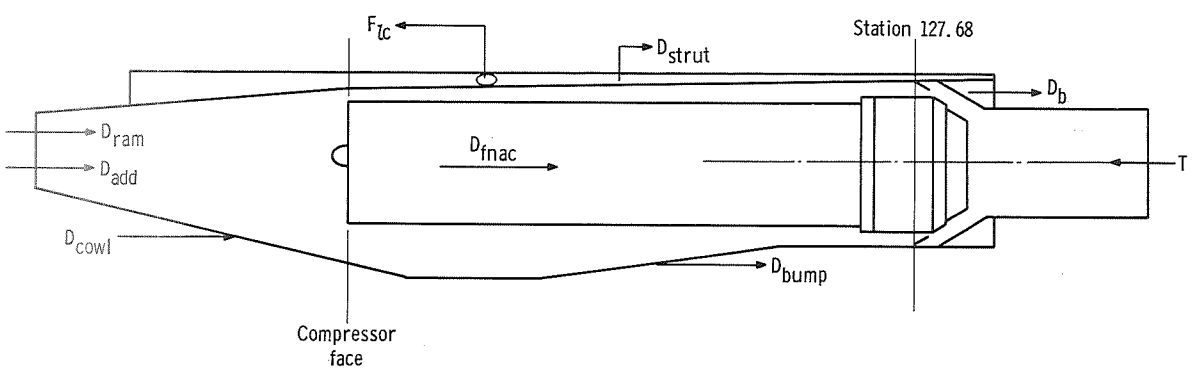

Figure 19. - Detailed nacelle forces.

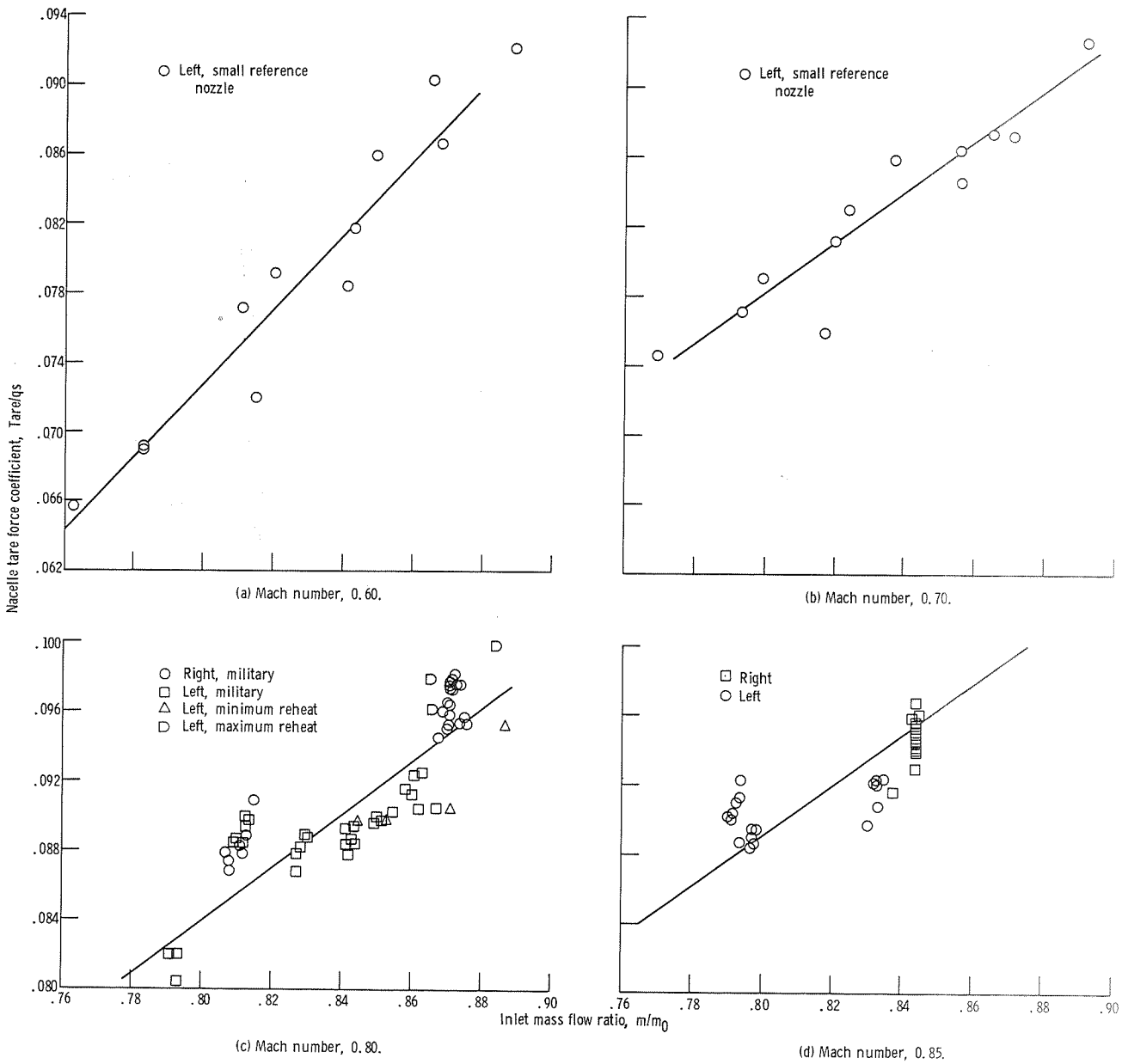

Figure 20. - Tare coefficient as a function of inlet mass flow ratio.

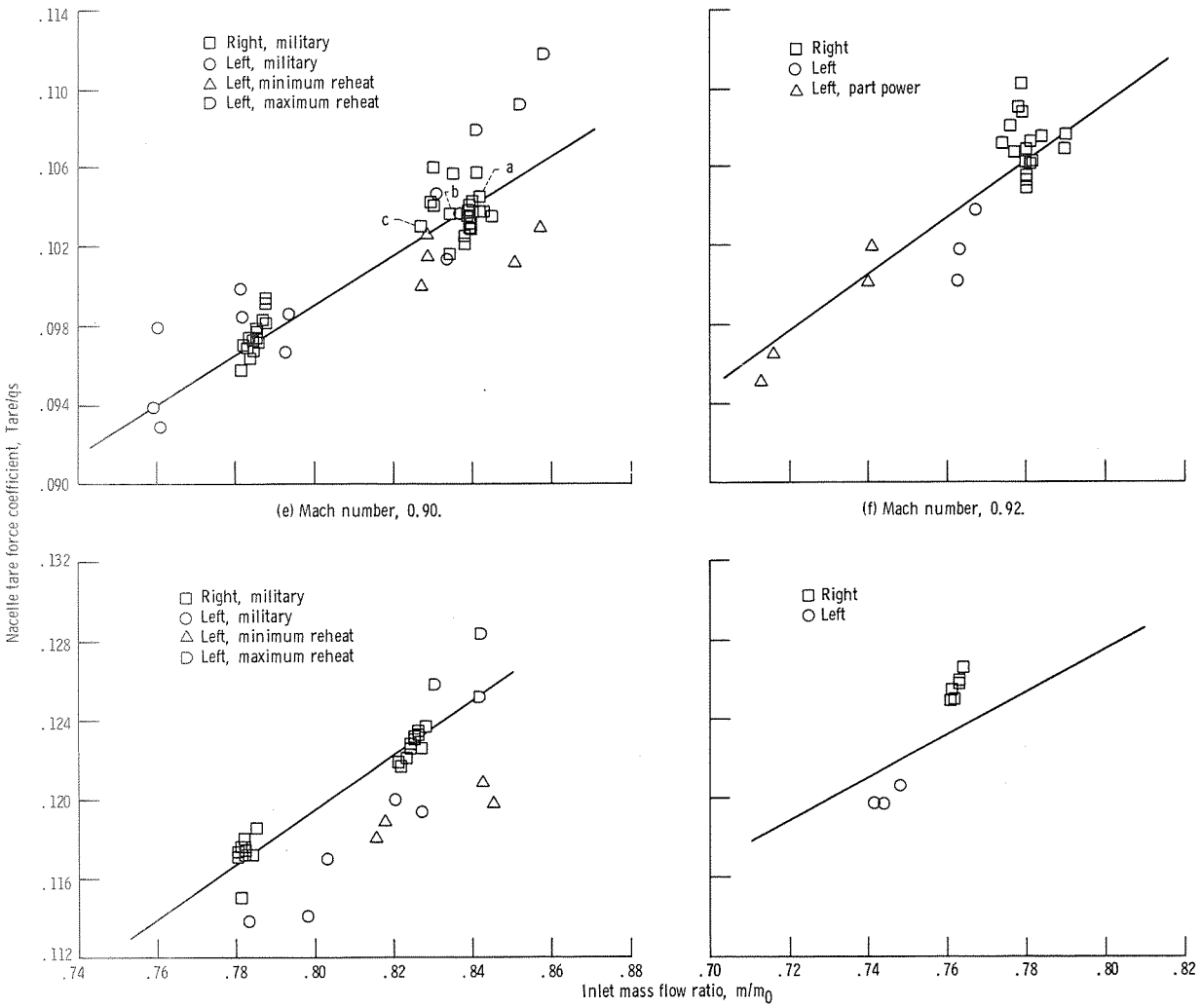

(e) Mach number, 0.90.

(f) Mach number, 0.92.

(g) Mach number, 0.95.

(h) Mach number, 1.06.

Figure 20. - Continued.

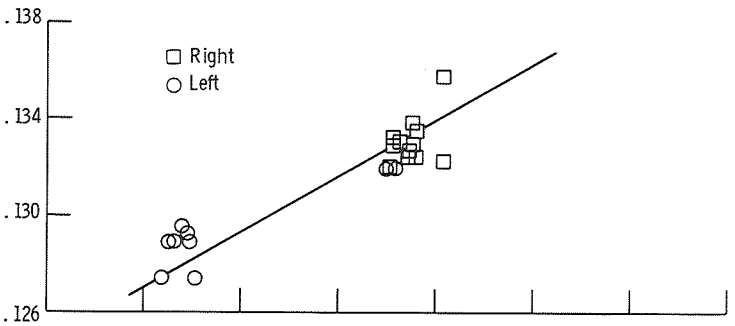

(i) Mach number, 1.10.

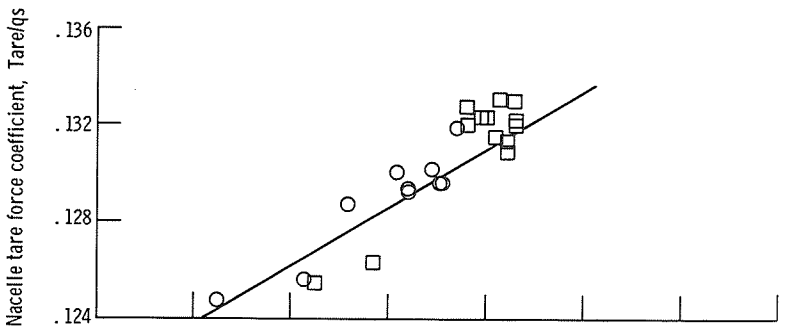

(j) Mach number, 1.20.

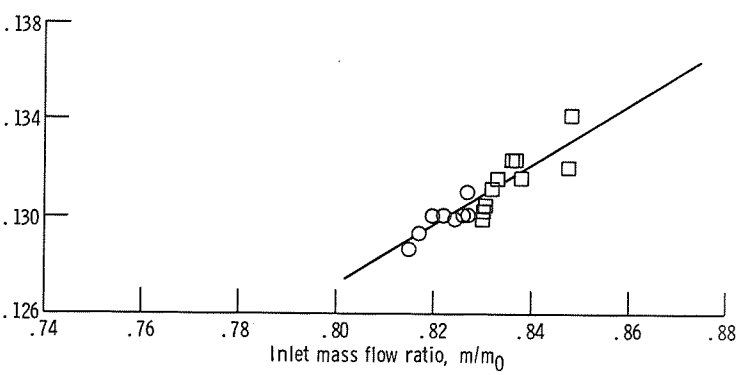

(k) Mach number, 1.30.

Figure 20. - Concluded.

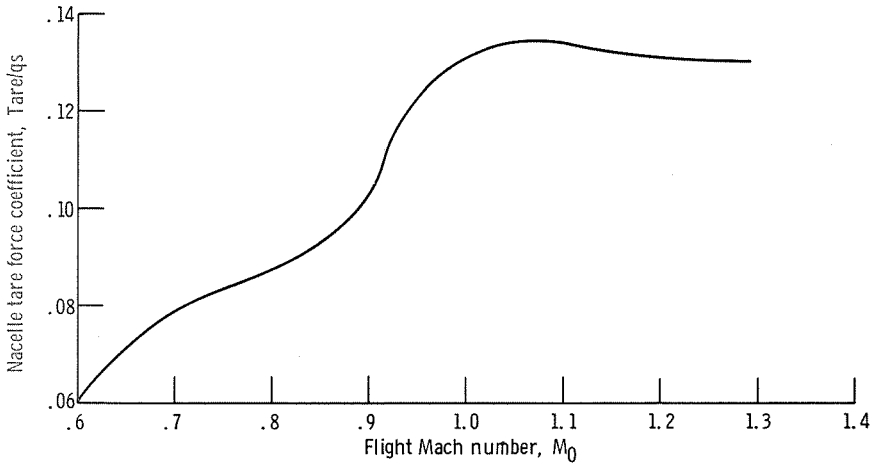

Figure 21. - Tare coefficient variation with Mach number at constant mass flow ratio of 0.82.

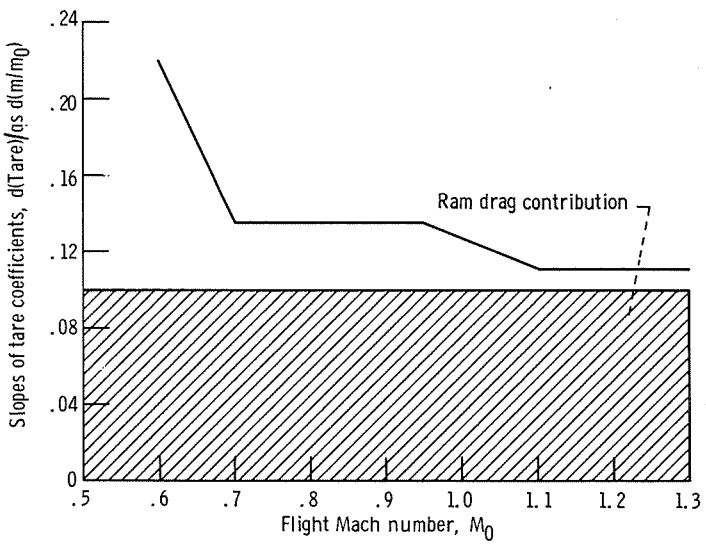

Figure 22. - Change of tare coefficient with mass flow ratio.

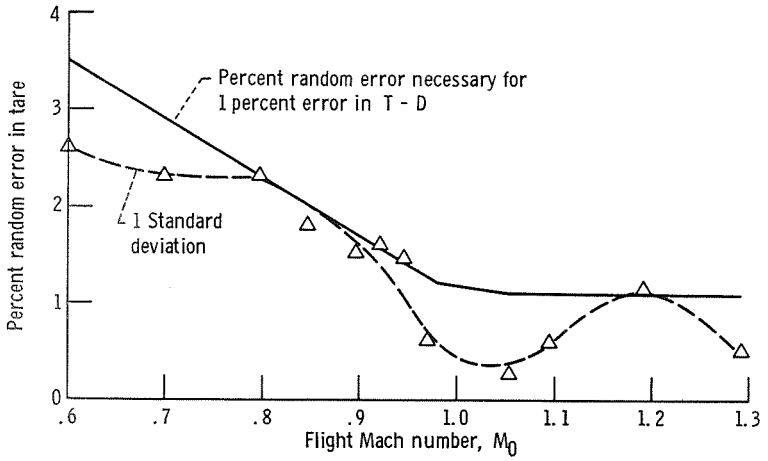

Figure 23. - Percent random error in tare as a function of flight Mach number for military power.

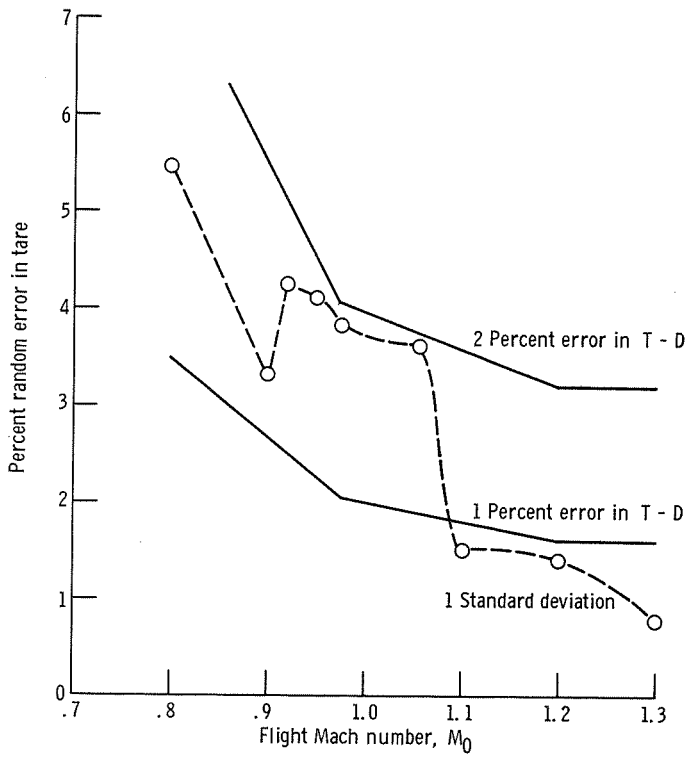

Figure 24. - Percent random error in tare as a function of flight Mach number for afterburning.

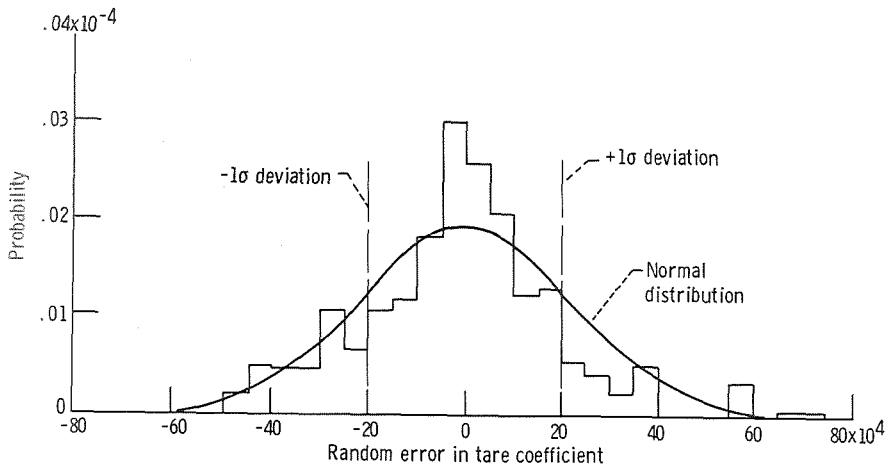

Figure 25. - Probability distribution of military data.

NASA-Langley, 1971 —— 28 E-5557

NATIONAL AERONAUTICS AND SPACE ADMINISTRATION
WASHINGTON, D. C. 20546

OFFICIAL BUSINESS
PENALTY FOR PRIVATE USE $300

FIRST CLASS MAIL

POSTAGE AND FEES PAID
NATIONAL AERONAUTICS AND
SPACE ADMINISTRATION

POSTMASTER: If Undeliverable (Section 158 Postal Manual) Do Not Return

"The aeronautical and space activities of the United States shall be conducted so as to contribute . . . to the expansion of human knowledge of phenomena in the atmosphere and space. The Administration shall provide for the widest practicable and appropriate dissemination of information concerning its activities and the results thereof."

—NATIONAL AERONAUTICS AND SPACE ACT OF 1958

NASA SCIENTIFIC AND TECHNICAL PUBLICATIONS

TECHNICAL REPORTS: Scientific and technical information considered important, complete, and a lasting contribution to existing knowledge.

TECHNICAL NOTES: Information less broad in scope but nevertheless of importance as a contribution to existing knowledge.

TECHNICAL MEMORANDUMS: Information receiving limited distribution because of preliminary data, security classification, or other reasons.

CONTRACTOR REPORTS: Scientific and technical information generated under a NASA contract or grant and considered an important contribution to existing knowledge.

TECHNICAL TRANSLATIONS: Information published in a foreign language considered to merit NASA distribution in English.

SPECIAL PUBLICATIONS: Information derived from or of value to NASA activities. Publications include conference proceedings, monographs, data compilations, handbooks, sourcebooks, and special bibliographies.

TECHNOLOGY UTILIZATION PUBLICATIONS: Information on technology used by NASA that may be of particular interest in commercial and other non-aerospace applications. Publications include Tech Briefs, Technology Utilization Reports and Technology Surveys.

Details on the availability of these publications may be obtained from:

SCIENTIFIC AND TECHNICAL INFORMATION OFFICE

NATIONAL AERONAUTICS AND SPACE ADMINISTRATION

Washington, D.C. 20546